Recommendations for Field-Scale Induced Polarization (IP) Data Acquisition and Interpretation

Fardous Zarif[1,2], Pauline Kessouri[1] and Lee Slater[1]*
[1]Department of Earth & Environmental Sciences, Rutgers-Newark University, NJ 07102, USA
[2]Geophysical Exploration Department, Desert Research Center (DRC), Matarya 11753, Cairo
*Corresponding author

ABSTRACT

Field-scale induced polarization (IP) data remain underutilized due to the challenges of data acquisition and interpretation of the resulting observations for near surface environmental applications. We use measurements at a test site and the principle of IP reciprocity to demonstrate that the primary factor controlling the quality of IP data acquired using standard resistivity/IP imaging systems is the signal to noise ratio (SNR), *i.e.,* the recorded signal strength. This factor favors the use of nested arrays, where one or two of the potential electrodes fall between the current electrode pair, that guarantee a high primary voltage (V_p) versus Dipole-Dipole type arrays where voltage differences rapidly decay away from the current injection pair. Comparison of data acquired using stainless steel, Cu-$CuSO_4$ porous pot and graphite electrodes demonstrates that electrode material is a significant second order factor but only for measurements where the SNR is relatively low (for the instrument used in this study when $V_p < 30$ mV). We also propose a simple framework for interpretation of environmental IP datasets whereby the acquisition of IP data is used to remove the inherent ambiguity in the interpretation of standalone resistivity data such that the subsurface distribution of the surface conductivity and electrolytic conductivity contributions to the total conductivity can be resolved. We demonstrate this approach on a field site within a first order catchment where a high surface area formation likely limits vertical transport and promotes interflow. Sharp contrasts in electrical structure between the two slopes of the catchment are observed.

Introduction

Induced polarization (IP) is a mature geophysical method that was originally developed for mineral exploration (Seigel *et al*., 2007). Environmental applications of the method were first recognized in the late 1950s (Marshall and Madden, 1959; Vacquier *et al*., 1957; Wait, 1959). Interest in the environmental applications of the method has grown in the last twenty years as a result of laboratory measurements that have confirmed that additional information on subsurface properties and processes can be obtained relative to electrical resistivity measurements alone. Induced polarization effectively extends the conventional field-scale resistivity measurement by providing some information on the low frequency polarization of the porous medium in addition to the conductivity of the medium provided by a standard electrical resistivity measurement. Field measurements are most commonly acquired in the time domain (TDIP) where the decay of a transient voltage is recorded shortly following current shut off. However, field measurements can also be acquired in the frequency domain, where the phase lag is recorded between the induced voltage and applied current for a sinusoidal waveform.

Multi-channel electrical resistivity acquisition systems now permit large numbers of data to be acquired using multiple electrode arrays. Most of these systems offer the opportunity to simultaneously acquire TDIP data. Whereas reliable resistivity data are relatively straightforward to acquire, the acquisition of reliable IP data is not requiring careful consideration of data acquisition parameters selected by the operator. Without such attention to detail, IP data are routinely noisy and/or inconsistent with the physics of the underlying IP mechanisms. There are numerous factors that contribute to this problem, but the primary factor is the much smaller signal to noise ratio (SNR) associated with the IP measurement relative to the resistivity measurement in environmental applications. The SNR is often 100–1,000 times smaller for IP relative to resistivity measurements

 DOI: #10.2113/JEEG22.4.395

for environmental applications. Consequently, IP data are often acquired but subsequently discarded based on poor data quality. Far worse, interpretation (*e.g.,* from inversion and imaging) of poor quality IP data will result in misinterpretation of subsurface structures and processes. This problem is confounded by the fact that environmental applications of the IP method often rely on the detection of small changes in polarization of the subsurface relative to what is recorded in mineral exploration (Slater and Lesmes, 2002).

The interpretation of field-scale IP data also presents challenges. Unlike the electrical resistivity measurement, the link between the IP measurement acquired with field instruments and the subsurface physical properties is not straightforward (Lesmes and Frye, 2001). Furthermore, laboratory experiments have highlighted a large array of possible factors that can change the polarization of the subsurface, giving the impression of substantial ambiguity in the interpretation of images of IP structures.

In this paper, we present recommendations for acquisition of field-scale IP data using standard electrical imaging systems. We focus on the acquisition of a single measurement of the strength of the subsurface polarization (average chargeability) as this is the primary piece of information obtained with such instrumentation and this alone presents substantial challenges in acquisition. The considerations presented here will also apply to recent developments of the method that attempt to extract more subsurface information, *e.g.,* from the collection of full waveform IP data (Fiandaca *et al*., 2013, 2012), or the acquisition of spectral IP data by making measurements over a range of frequencies (Kemna *et al*., 2014). We use a well characterized test site to demonstrate key considerations for data acquisition: electrode configurations, electrode type and injection parameters. We also discuss the value of field-scale IP data in resolving the inherent ambiguity in the interpretation of resistivity data alone where the competing effects of electrolytic conduction through the interconnected pore space and surface conduction in the electrical double layer cannot be resolved. We demonstrate our methodology using results from a Critical Zone Observatory (CZO) where the IP data acquired help to determine contrasting geological controls on catchment hydrogeology and provide evidence for a geological unit that impedes vertical flow and transport.

The IP Measurement

The IP measurement is made using a standard four electrode array where current is injected across a dipole and the resulting voltage difference is recorded across a second dipole (Fig. 1). The IP effect manifests itself as a residual voltage following termination of an applied current (time domain measurement), as a frequency dependent resistivity (percent frequency effect, PFE) or as a phase lag (φ) between the voltage waveform and the current waveform. These measurements are equivalent in that they can be shown to describe the ratio of the polarizability to the conductivity of the subsurface (*e.g.,* Slater and Lesmes, 2002).

The most common measurement of the magnitude of the IP effect in the time domain is the chargeability M (*e.g.,* Telford *et al*., 1990),

$$M = \frac{\int_{t_s}^{t_f} V_s dt}{V_p} \frac{1}{\Delta t}, \quad (1)$$

where V_s is a residual voltage integrated over a time window defined between times t_s and t_f after termination of an applied current, V_p is the measured voltage at some time during application of the current and Δt equals the length of the integrated time window (Fig. 1). Units of chargeability are typically quoted as millivolts per volt (mV/V) recognizing that the IP measurement is often 100–1,000 times smaller than the resistivity measurement determined using V_p alone. Given that this is the most commonly measured field parameter, we focus our analysis on measurements of M, although the same considerations would apply when measuring PFE or φ in the field.

Interpretation of the IP Measurement

Understanding the significance of IP measurements requires a basic understanding of charge transport mechanisms in porous media and the physical properties that control the ability of a material to transport electric charge via these mechanisms. Charge transport phenomena can be represented as a measured resistivity, conductivity or dielectric permittivity. Over the last twenty years, electrical conductivity terminology has been selected to establish the required link between physical property and measurement within the IP community (Kemna *et al*., 2012). The extension of the measured electrical conductivity to also represent measured polarization needed to interpret IP data is done via a measured complex electrical conductivity (σ^*), where the real (σ') and imaginary (σ'') components of σ^* represent respectively conduction (electromigration of charges under the influence of an electric field) and polarization (reversible storage of charges under the

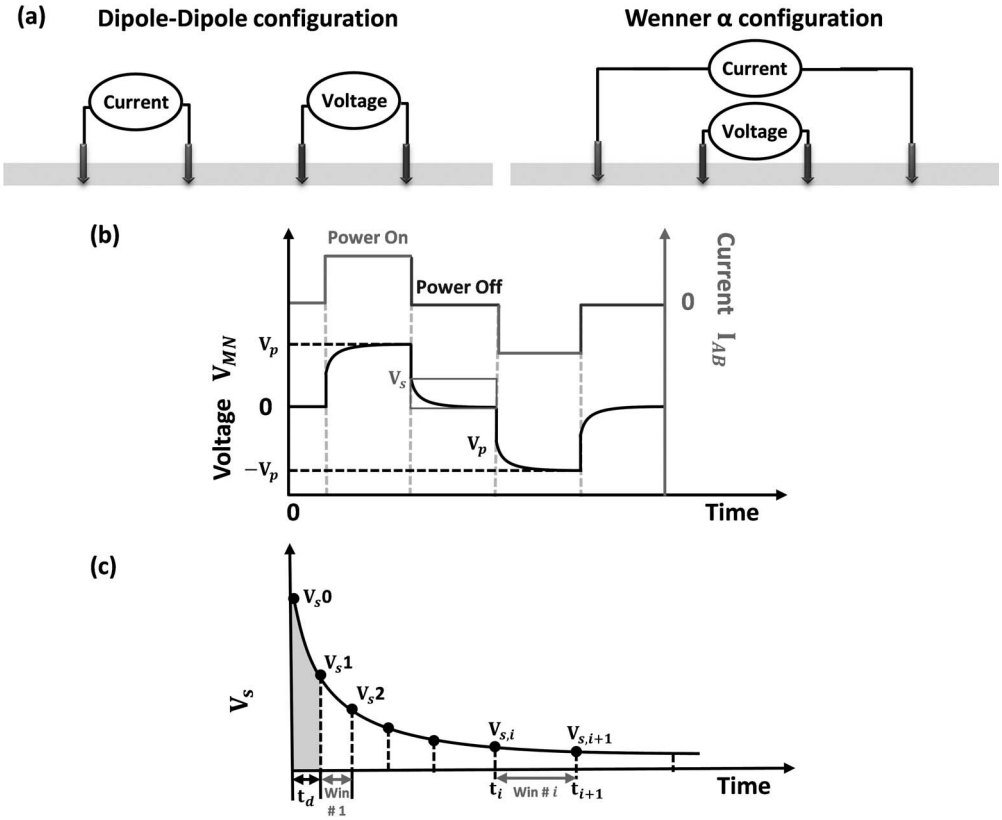

Figure 1. (a) Dipole-Dipole and Wenner α electrode configurations; (b) classical current transmission waveform and resulting voltage recorded in the presence of an IP effect showing the primary V_p and secondary V_s voltage; (c) typical sampling of the decay curve showing integrals used to compute the chargeability and the delay time (t_d).

influence of an electric field) mechanisms. In the standard resistivity measurement only the magnitude of the complex electrical conductivity ($|\sigma^*|$) is recorded. Given that polarization is typically 100–1,000 times less than conduction,

$$|\sigma^*| \cong \sigma' \tag{2}$$

Models for the low frequency (*e.g.,* less than 100 Hz) complex conductivity of a porous medium are based on assuming charge transfer occurs via two parallel mechanisms: (i) electrolytic conduction, without any polarization, through the interconnected pore space represented by the electrolytic conductivity σ_{el}, and (ii) charge transfer including both conduction and polarization associated with charges in the electrical double layer (EDL) at the interfaces of the interconnected pore surface via the surface conductivity ($\sigma_{\text{surf}}{}^*$) (*e.g.*, Vinegar and Waxman, 1984),

$$\sigma^* = \sigma_{el} + \sigma_{\text{surf}}{}^* \tag{3}$$

As the electrolyte is essentially unpolarizable at low frequencies, electrolytic conduction is a purely real term so the imaginary component of the measured complex conductivity is solely related to the surface polarization,

$$\sigma'' = \sigma_{\text{surf}}{}'' \tag{4}$$

whereas the measured real part of the complex conductivity depends on both the electrolytic and the surface conduction,

$$\sigma' = \sigma_{el} + \sigma_{\text{surf}}{}' \tag{5}$$

The electrolytic conductivity can be related to the properties of the saturated interconnected pore space and the pore filling fluid conductivity (σ_w) via Archie's Law (Archie, 1942),

$$\sigma_{el} = \sigma_w . \varphi_{int}{}^m \tag{6}$$

where φ_{int} is the interconnected porosity and m is a cementation factor related to the tortuosity. Returning back to the IP measurements, we recount that (i) $M \cong \varphi$ (Slater and Lesmes, 2002), and (ii) polarization is typically much smaller than conduction such that,

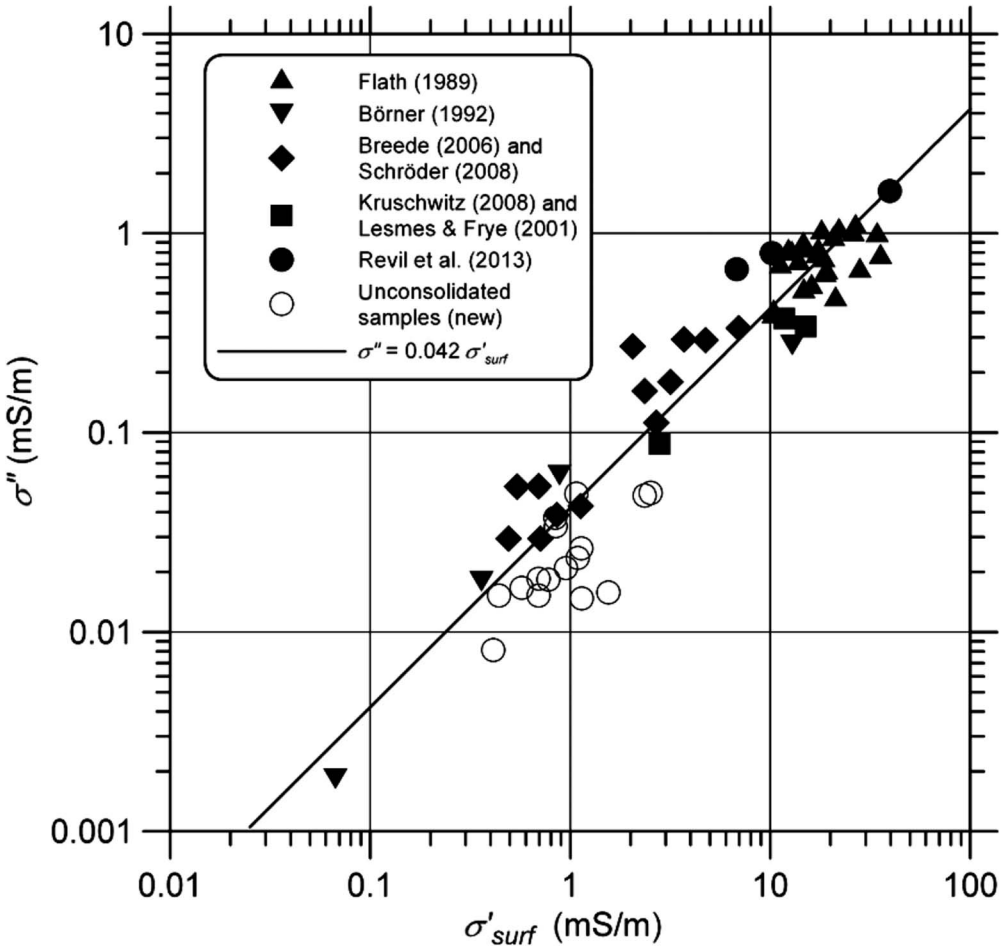

Figure 2. The dependence of imaginary conductivity ($\sigma'' = \sigma_{surf}''$) on surface conductivity (σ_{surf}') at 1 Hz reproduced from Weller *et al*. (2013). The best-fit line shows the single linear fit to the entire data set where $l = 0.042$ with $R^2 = 0.911$.

$$M \cong \varphi = \tan^{-1}\left(\frac{\sigma''}{\sigma'}\right) \cong \frac{\sigma''}{\sigma'} = \frac{\sigma_{surf}''}{\sigma_{el} + \sigma_{surf}'} \qquad (7)$$

$(\varphi < 100\,\text{mrad}$ for enviromental applications$)$

Consequently, it is clear that the measured IP effect M represents the polarization strength relative to the conduction strength in a porous material.

One common misinterpretation of field IP datasets is to assume that M represents a direct measurement of the polarization strength. As shown by Eq. 7, M will vary with both the polarization and the conduction occurring in the sample. Emphasizing again that polarization is typically 100–1,000 times smaller than conduction (Eq. 2), a direct measurement of the polarization known as the normalized chargeability (M_n) can be directly computed from the field measurements,

$$M_n = M \cdot |\sigma| \cong \varphi.\sigma' \cong \sigma'' = \sigma_{surf}'' \qquad (8)$$

The traditional ambiguity of resistivity interpretation is highlighted by Eq. 5, which shows that the acquired single measurement ($|\sigma^*| \cong \sigma'$) is the sum of electrolytic (σ_{el}) and real surface (σ_{surf}') conductivity. Equation 8 highlights that the additional measurement of IP provides a direct estimation of the surface polarization (σ_{surf}''). A direct linear relationship between σ_{surf}'' and σ_{surf}' was first proposed by (Börner *et al*., 1996) and experimentally verified with a large database by Weller *et al*. (2013), as shown in Fig. 2:

$$\sigma'' = \sigma_{surf}'' \cong 0.042 * \sigma_{surf}' \qquad (9)$$

Consequently, the acquisition of IP data has the potential to remove the ambiguity in the interpretation of traditional resistivity data by directly resolving the surface conductivity.

From the complex conductivity σ^* measured in the field, using Eqs. 4, 5 and 9, we can separate the effects of the electrolytic conductivity and the real surface conductivity through:

$$\sigma_{el} = \sigma' - \sigma_{\text{surf}}{}' \cong \sigma' - \sigma''/0.042 \qquad (10)$$

The interest in IP has been stimulated by the fact that surface conduction and polarization are sensitive to geometrical and geochemical properties of the mineral-fluid interface. The strong dependence of σ'' on the total pore-normalized internal surface area (S_{por}) is well recognized (*e.g.,* Börner, 1992; Weller *et al*., 2013). In contrast, the dependence of σ'' on σ_w is relatively weak (Weller and Slater, 2012) such that σ'' is generally considered an excellent indicator of lithologic variability. Given that S_{por} is a proxy measure of the inverse hydraulic radius, substantial work has focused on the estimation of permeability (k) from IP measurements (*e.g.,* Binley *et al*., 2005; Kruschwitz *et al*., 2010; Revil and Florsch, 2010; Slater and Lesmes, 2002; Titov *et al*., 2010; Koch *et al*., 2011; Revil *et al*., 2015, 2014). Much laboratory research has recently focused on the sensitivity of IP measurements to changes in the geometrical and geochemical properties of the mineral-fluid interface driven by a variety of geochemical and biogeochemical processes (*e.g.,* Atekwana and Slater, 2009; Atekwana and Atekwana, 2010; Heenan *et al*., 2015; Ntarlagiannis *et al*., 2016; Revil *et al*., 2010). Although intriguing, and suggesting potential future applications of IP in subsurface monitoring, these signals are mostly small and challenging to reliably record with field-scale time domain IP instruments. Perhaps then, the most powerful utilization of field-scale IP datasets is foremost to improve resistivity imaging interpretation by resolving the electrolytic and surface conductivity, which cannot be done with resistivity data alone. We focus on this application here.

Data Acquisition Considerations

Common considerations when conducting IP surveys include the choice of electrode array and the choice of electrode material. Historically, the mining IP community developed the IP method favoring the use of the classic Dipole-Dipole configuration and the application of non-polarizing porous pot (*e.g.,* Cu-$CuSO_4$) electrodes for recording data on the potential electrode pairs (dipole) (*e.g.,* Bleil, 1953; Polyakov, 1951; Sumi, 1959). These choices were made to limit polarization of the potential recording electrodes that was a source of significant noise in the data. Porous pots maintain an equal potential difference between the metal of the electrode and the ionic solution in the pot for both electrodes.

Dipole-Dipole arrays are arranged so that a 2D survey line is acquired without needing to occupy an electrode previously used for current injection (charging up that electrode) as a potential recording electrode. Such considerations were necessary given the state of development of IP instrumentation prior to the advent of modern electrical imaging systems that perform automatic processing of the data to calculate the residual voltage due to electrode polarization across the potential pair. Today's resistivity/induced polarization systems adequately compensate for the residual polarization of the potential electrodes such that non-polarizing electrodes are not a requirement as demonstrated by Dahlin *et al*. (2002) for a systematic study of the comparison of IP data quality for porous pots versus conventional stainless steel electrodes.

One additional consideration when collecting IP data is that, when using time domain instrumentation, the time required to collect each resistivity and IP data point is greater than when collecting resistivity data alone. This additional time will partly depend upon the nature of the subsurface. For example, coarse-grained materials are characterized by slower decays that may require longer time windows to adequately record. The time period used to inject current (Fig. 1(b)) may need to be reevaluated after initial assessment of measured decay curves.

A primary factor controlling IP data quality with modern imaging systems is the signal to noise ratio (Gazoty *et al.,* 2013). Whereas resistivity measurements are calculated from the primary voltage (V_p), a reliable IP measurement requires an accurate recording of $\int_{t_s}^{t_f} V_s\, dt$, where V_s is typically 100–1,000 times less than V_p. Consequently, primary factors for the acquisition of reliable IP data include the contact resistance at the current electrodes limiting current injection and the use of array configurations that result in a high SNR. The use of Dipole-Dipole arrays as historically done is inconsistent with the latter requirement as the primary voltages on the potential electrode pairs rapidly decrease with distance from the current injection pair. Instead, nested arrays, where one or two of the potential electrodes fall between the current electrode pair, increase the SNR and will improve IP data quality. We demonstrate such concepts below, using reciprocal measurements (where the current and potential electrode pairs are swapped) as a robust measure of IP data quality in the same way as they are used to evaluate resistivity data quality (Slater *et al*., 2000). Gazoty *et al*. (2013) previously demonstrated the overarching importance of SNR to IP measurements based on repeatability tests, but at the same time acknowledged that repeatability is not a robust measure of data quality in field-scale measurements. Our tests based on reciprocity also highlight the

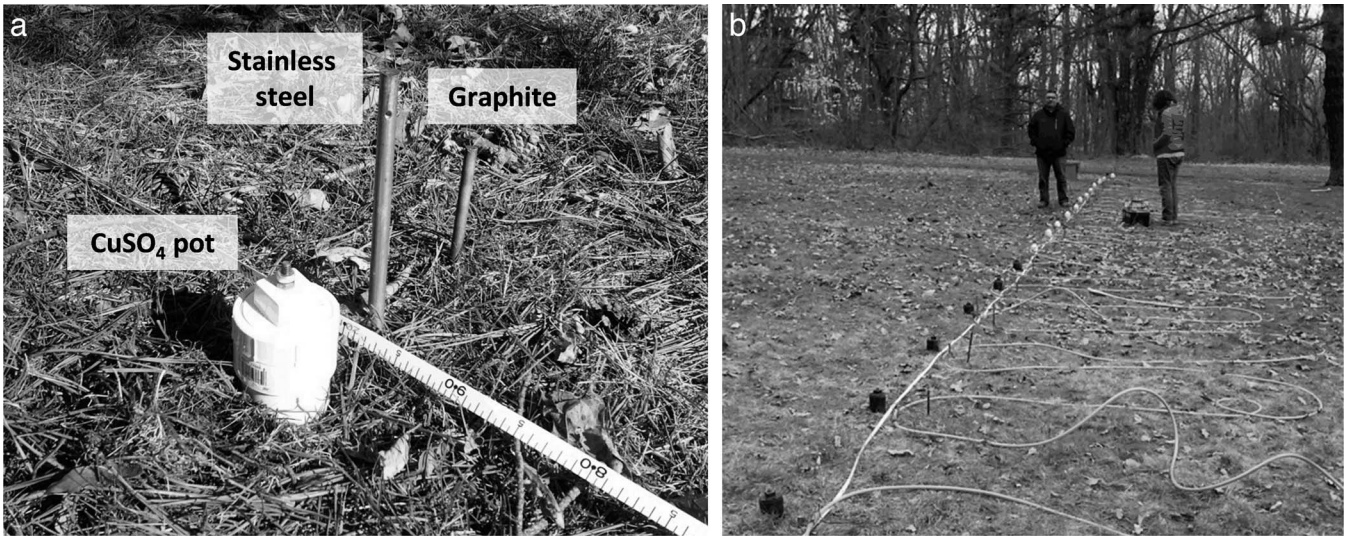

Figure 3. (a) close up of the three electrodes (stainless-steel, graphite and Cu-$CuSO_4$ porous pot) at all 24 electrode locations; (b) 24 electrode array at test site.

second order effects on IP data quality associated with electrode material.

Methods

Test Site

We made use of a test site local to Rutgers University Newark (New Jersey, USA) to demonstrate key considerations when acquiring IP data. The site is a small park where about 11 m of unconsolidated glacial deposits overly the bedrock. The site is flat, grass covered and completely devoid of any infrastructure. A 2D survey composed of 24 electrodes with a 1 m separation was laid out on the site. Measurements were acquired using three types of electrodes: (1) stainless steel rods; (2) Cu-$CuSO_4$ porous pots; (3) graphite (Fig. 3). The latter was included as our laboratory spectral induced polarization measurements have indicated that graphite may be a lower noise (*i.e.*, less polarizable) electrode than stainless steel. Good performance of graphite electrodes has been previously reported for standard resistivity measurements (Van Dam *et al*., 2009). Measurements were acquired with a Dipole-Dipole array and a Wenner α array, the most common nested array configuration. Contact resistances were recorded on all electrodes prior to the start of each sequence of measurements. All data were acquired with an Iris Syscal Pro resistivity/induced polarization meter with a common set of transmitter parameters: 2 second on-off waveform; 400 V transmitter voltage; 2 stacks for each measurement; 20 IP windows each of length 80 ms and a 240 ms delay. Full reciprocal measurements were acquired in order to characterize the noise levels in each measurement.

Garner Run

Resistivity and induced polarization measurements were acquired at Garner Run, a first-order catchment within the Shavers Creek watershed in central Pennsylvania. Garner Run is characterized as a synclinal valley underlain by the Silurian Tuscarora Formation between NW–SE trending ridges of Tussey Mountain and Leading Ridge (Brantley *et al.,* 2016). The catchment experienced periglacial conditions in the Last Glacial Maximum and shallow coring showed that the valley is largely filled by quartz sand. The Tuscarora formation mostly consists of pure quartz sandstone with minor interbedded shales, and is considered the ridge-forming unit that caps the highest topography in Shavers Creek watershed.

It is often difficult to understand hydrologic processes in such upland catchments where the subsurface architecture is largely unknown. Geochemical data acquired from a nest of wells in the stream bed suggest that both shallow interflow and deeper groundwater contribute to stream flow. The objective of the survey was to assist in the interpretation of the subsurface hydrogeological framework of the catchment, with a specific focus on identifying evidence for low permeability confining layers that might limit vertical transport and promote shallow interflow towards the stream.

The initial survey consisted of a 480 m 2D resistivity imaging line with stainless steel electrodes spaced 2 m apart. Resistivity data were acquired with a

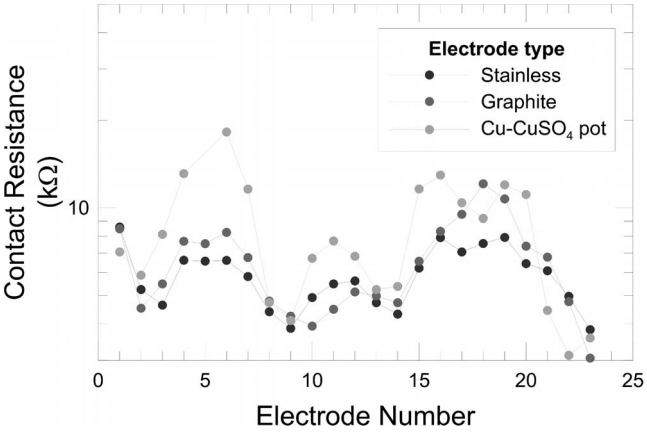

Figure 4. Contact resistances measured for the three electrode materials used: stainless steel, graphite and porous pot filled with $CuSO_4$.

mixed array data acquisition sequence that consists of a combination of array types including short-offset Dipole-Dipole (using multiple electrode spacings), and Wenner α configurations, both providing a high SNR. A total of 3,518 measurements were acquired with 1,614 additional reciprocal measurements used to quantify error levels at the site and to develop an error model for inversion of the dataset. IP data were not acquired on this large-scale survey due to time constraints. However, interpretation of this survey line revealed a striking difference in the electrical structure between two sides of the catchment, and follow up IP surveys were subsequently conducted on two sections of the initial line in order to constrain interpretation of the imaged structures. These IP surveys were performed on two lines situated at locations that emphasized the differences in the electrical resistivity structure on either side of the catchment. Each line consisted of 48 electrodes spaced 2 m apart. A total of 895 IP measurements (727 normals plus 168 reciprocals for error analysis) were acquired on each line using a mixed array data acquisition sequence (combination of array types including short-offset Dipole-Dipole, Wenner α, and "skip-two" (a dipole length of three electrodes) Dipole-Dipole configurations). This sequence, previously developed for IP data acquisition (Mwakanyamale *et al*., 2012), consistently results in an adequate SNR ratio needed to ensure reliable IP measurements and also provides a sensitivity pattern that compares favorably against other standard configurations (Mansoor and Slater, 2007). Both lines were acquired with an Iris Syscal Pro resistivity/induced polarization meter with a common set of transmitter parameters: 2 second on-off waveform; 400 V transmitter voltage; 2 stacks for each measurement; 20 IP windows each of length 80 ms and a 240 ms delay.

Results

Test Site Results

Results from the test site highlight the dependence of IP data on SNR and electrode material. Considering first the issue of electrode material, Fig. 4 shows contact resistances measured between two consecutive electrodes for the three tested electrode types. The measurements show that contact resistances do vary as a function of electrode type. The stainless steel and graphite electrodes have near identical contact resistances whereas the Cu-$CuSO_4$ porous pots are characterized by some higher contact resistances (up to twice that of the stainless steel and graphite electrodes at some locations along the line). Although the surface of the electrode in contact with the ground is higher than for the stainless steel and the graphite electrodes, the metallic part of the electrode is not directly in contact with the ground, but indirectly through a super-saturated Cu-$CuSO_4$ solution and a porous wood end-cap.

Figure 5 shows the distribution of the chargeability reciprocal errors as a function of the primary receiver voltage (V_p in Fig. 1) for both the Dipole-Dipole (Figs. 5(a)–(c)) and Wenner α (Figs. 5(d)–(f)) arrays. Unlike resistivity data where errors are typically quantified as a percentage deviation, IP errors are better quantified as an absolute deviation, where reciprocity within 1 mV/V is considered a high quality measurement (Flores Orozco *et al*., 2012; Slater and Binley, 2006). Figure 5 illustrates that the majority of IP reciprocal errors are less than the 1 mV/V threshold in all cases. Figure 5 also highlights the difference in V_p, and thus V_s, between the Dipole-Dipole and Wenner α array configurations. Whereas all the primary voltages measured with the Wenner α array are above 100 mV/V, V_p varies from a few mV to 5,000 mV for the Dipole-Dipole array. The errors for the Dipole-Dipole array show a characteristic structure where they increase significantly below some minimum voltage, shown here for this specific instrument to be around $V_p = 30$ mV. This highlights a frequent limitation of the Dipole-Dipole array (Gazoty *et al*., 2013), especially at sites where (1) the electrical conductivity is high such that primary voltages are low, and (2) noise levels are more significant, *e.g.,* closer to any infrastructure. At our relatively resistive application site that is devoid of effects of any infrastructure, the Dipole-Dipole array performs quite well but is a function of electrode material as discussed below.

To examine the effects of the electrode, histograms of both resistivity and chargeability reciprocal errors for the three different electrode materials with all other acquisition parameters (survey type, transmitter and

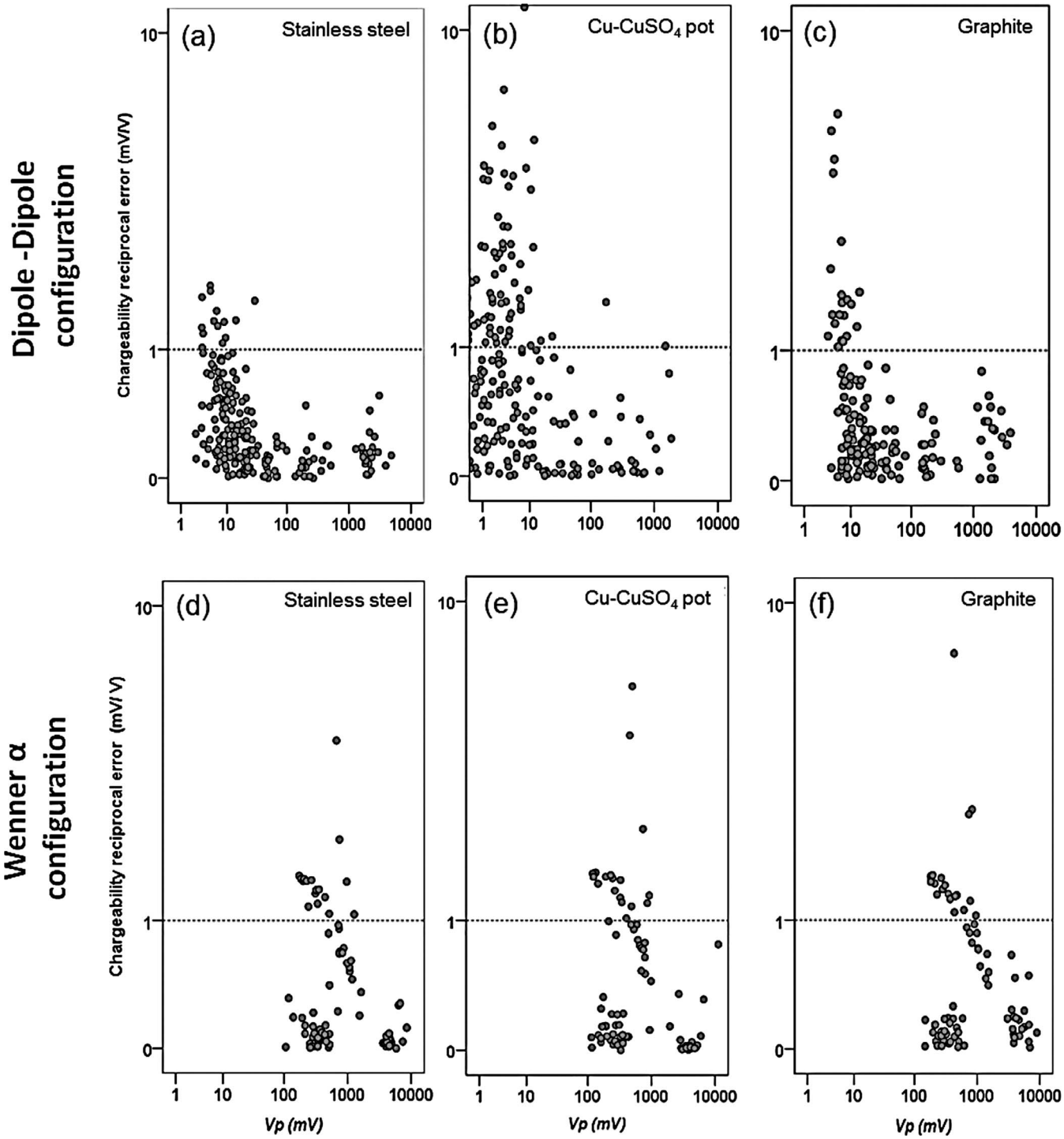

Figure 5. Distribution of IP reciprocal errors as a function of electrode array, electrode material and primary voltage (V_p): (a–c) Dipole-Dipole configuration for stainless steel, Cu-$CuSO_4$ porous pot and graphite electrodes respectively; (d–f) Wenner α configuration for stainless steel, porous pot and graphite electrodes, respectively. Dashed line denotes the 1 mV/V threshold above which IP measurements are discarded from the inversion. For the Dipole-Dipole array, 93%, 60% and 84% of the measurements are below the threshold for the stainless steel, Cu-$CuSO_4$ porous pot and graphite electrodes respectively. For the Wenner α array, 74%, 79% and 44% of the measurements are below the threshold for the stainless steel, Cu-$CuSO_4$ porous pot and graphite electrodes respectively.

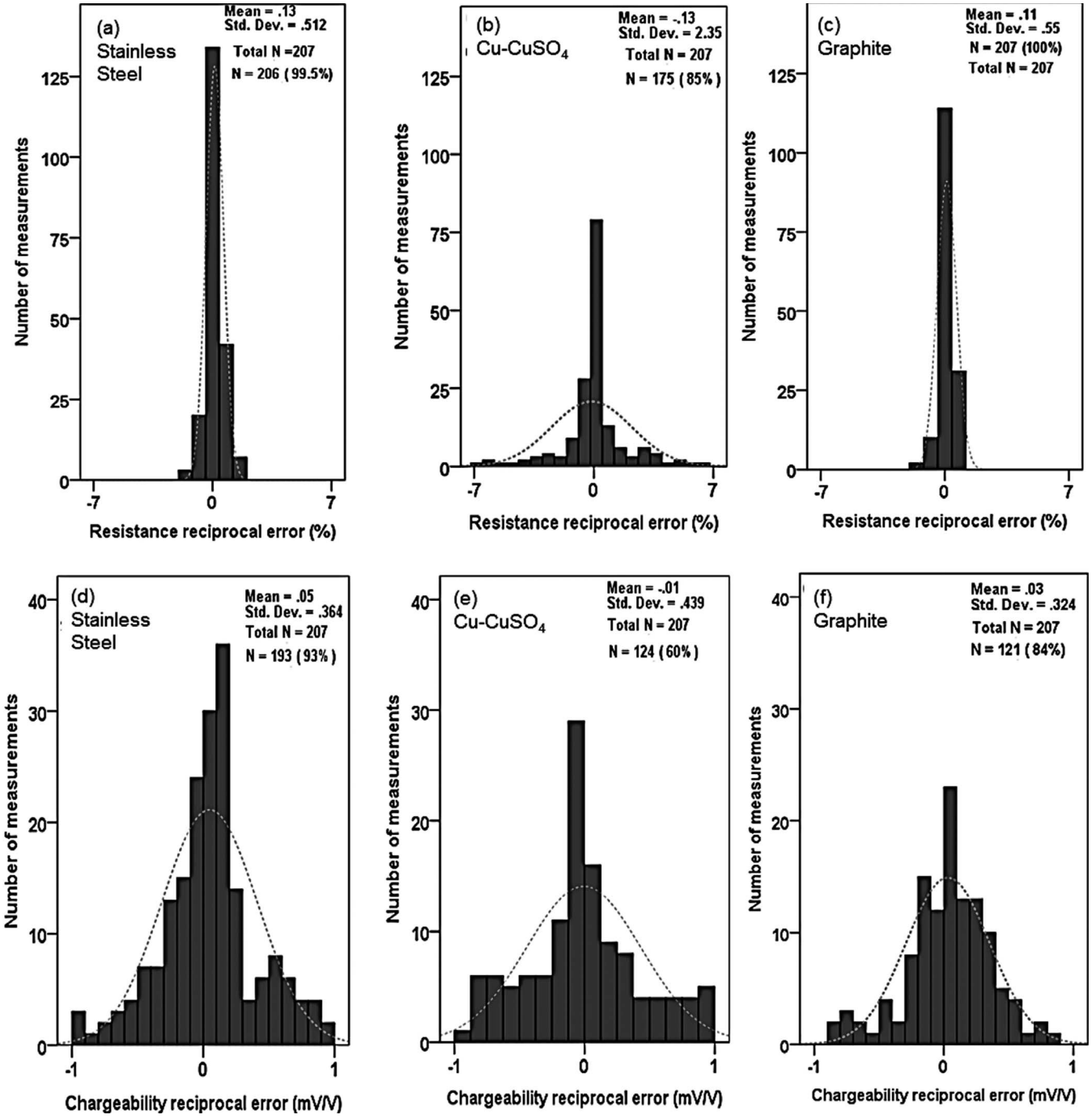

Figure 6. Histograms of reciprocal errors acquired using the Dipole-Dipole array: (a–c) percentage resistance errors for stainless steel, Cu-$CuSO_4$ porous pot and graphite electrodes respectively; (d–f) absolute chargeability errors for stainless steel, Cu-$CuSO_4$ porous pot and graphite electrodes respectively. Dashed lines represent fitted normal distributions with mean and standard deviation (std. dev.) shown in each case.

receiver settings) equal are shown for the Dipole-Dipole and Wenner α electrode configurations in Fig. 6 and Fig. 7, respectively. Considering the Dipole-Dipole configuration, Fig. 6 further highlights the effect of electrode material on data quality for the Dipole-Dipole configuration. For both resistivity and chargeability reciprocity, stainless steel electrodes perform better (based on number of data filtered out) than both the graphite and Cu-$CuSO_4$ arrays. This finding is also apparent in Figs. 5 (a)–(c). The Cu-$CuSO_4$ porous pots show the poorest

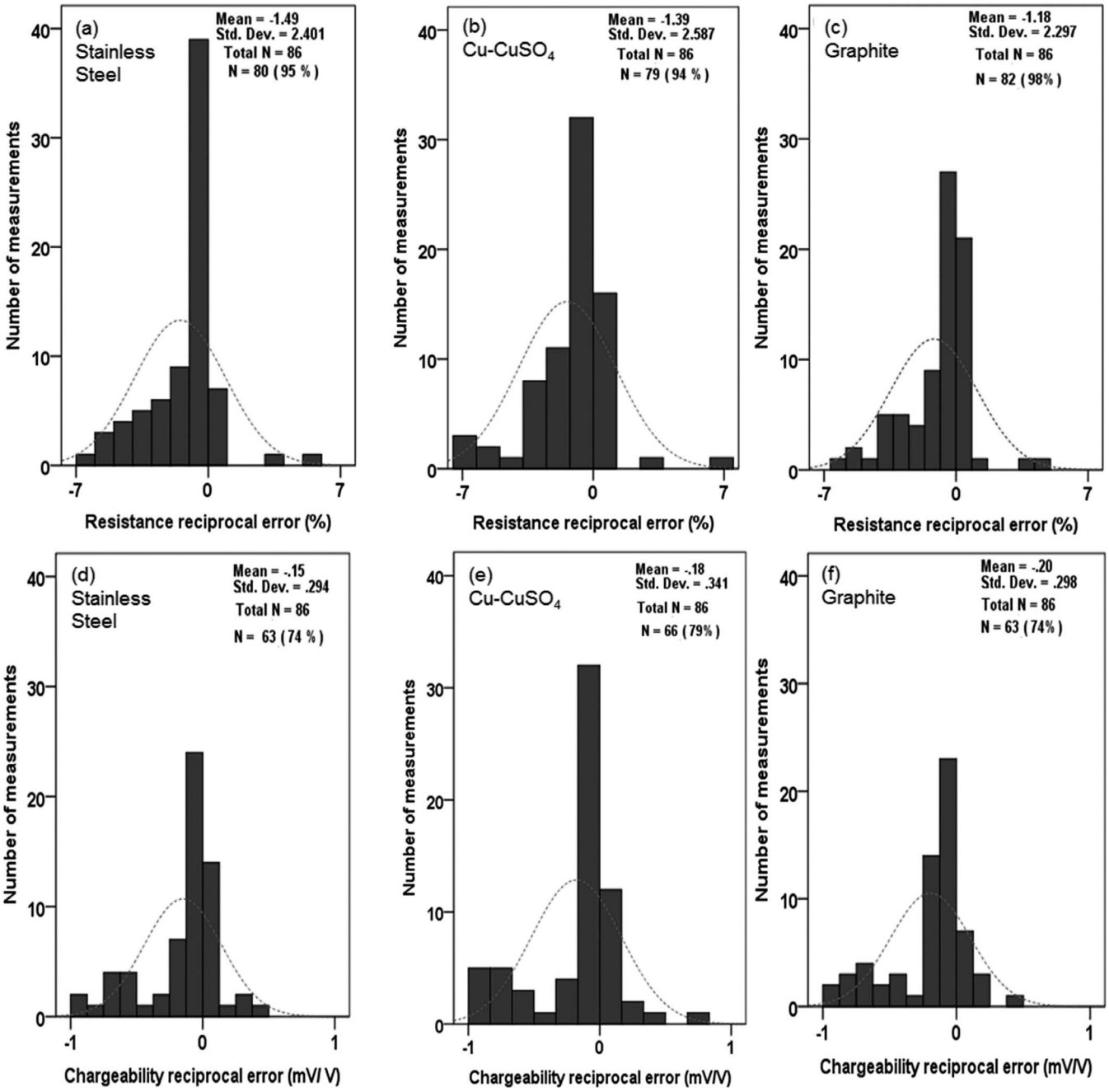

Figure 7. Histograms of reciprocal errors acquired using the Wenner α array: (a–c) percentage resistance errors for stainless steel, Cu-$CuSO_4$ porous pot and graphite electrodes respectively; (d–f) absolute chargeability errors for stainless steel, Cu-$CuSO_4$ porous pot and graphite electrodes respectively. Dashed lines represent fitted normal distributions with mean and standard deviation (std. dev.) shown in each case.

data quality, with only 60% of the data passing the 1 mV/V reciprocity threshold. The poorer results with the Cu-$CuSO_4$ electrodes are likely in part a result of the higher contact resistances relative to the stainless steel and graphite electrodes (Fig. 4). In contrast, 93% and 84% of the data pass the 1 mV/V reciprocity threshold for the stainless steel and graphite electrodes respectively. Figure 7 shows that the differences in reciprocity between electrode materials disappear in the case of the Wenner α array, with near identical resistivity and chargeability error distributions (Figs. 7(d)–(f)) and percentages of measurements meeting the 1 mV/V threshold. This suggests that the effect of electrode material may only be important for the measurements

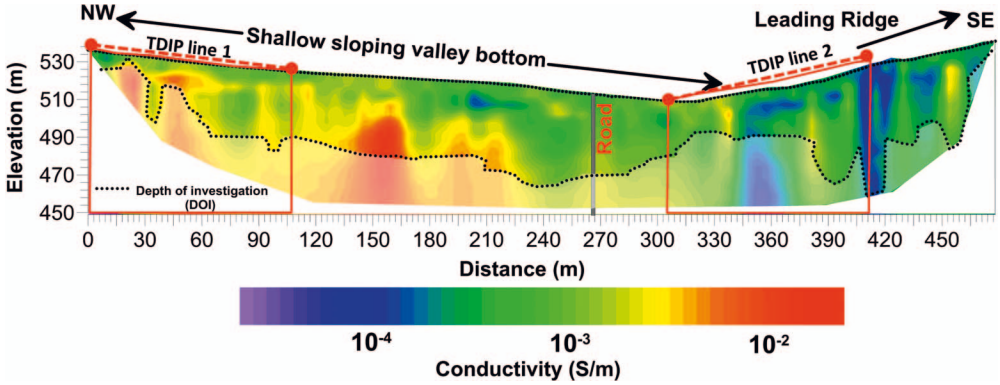

Figure 8. Image of conductivity distribution resulting from a 480 m roll-along survey across Garner Run (PA) showing contrasting conductivity structure between the shallow slope to the NW and the leading ridge to the SE. The two boxes represent the portions of the cross-section imaged with TDIP. The Depth of Investigation (DOI) calculated based on Deceuster *et al*. (2014) is shown as a limit on reliable structure in the image (the semi-transparent structure below the DOI is considered poorly constrained by the data).

with a smaller primary voltage V_p. This observation is also clearly illustrated in Fig. 5.

Garner Run Results

Figure 8 shows the 2D resistivity image for the inversion of the initial resistivity survey across the valley that motivated the follow up IP survey. The resistivity inversion highlights a strong contrast in electrical structure between the NW shallow slope and the SE leading ridge. The NW shallow slope shows evidence of a high conductivity unit overlain by a layer of moderate resistivity. The leading ridge is characterized by much lower conductivity with no evidence of an underlying high conductivity unit. This image was interpreted to indicate the possible presence of a prominent lithological contact between coarser sediments and an underlying fine-grained unit on the NW slope: this contact was interpreted to be an important hydrogeological interface limiting vertical transport and driving interflow towards the stream.

Figure 9 shows the analysis of the reciprocal errors acquired at Garner Run on IP lines TDIP1 and TDIP2 for 168 of 895 total measurements. Resistivity and IP data quality are high using the mixed array, with 95% of the IP reciprocals acquired passing the 1 mV/V filter threshold. Accurate quantification of data errors is a critical requirement to minimize artifacts and generate meaningful subsurface structures from resistivity data (LaBrecque *et al.,* 1996; Slater *et al*., 2000). Error models for the inversion, which were computed using a binning procedure first proposed by Koestel *et al*. (2008) for resistivity data alone and subsequently applied to IP data (Mwakanyamale *et al.,* 2012), are shown in Figs. 9(c)–(d). The IP error model is shown as an equivalent phase computed from the chargeabilities based on a laboratory calibration of the linear relationship between the chargeability from the Iris Syscal Pro (with settings as per this study) and the phase directly recorded using a laboratory spectral induced polarization instrument (PSIP by Ontash and Ermac, New Jersey, USA). The error models described by the fitting equations provide error estimates for all of the 895 measurements on the assumption that reciprocal errors computed for the 168 measurements are representative of the entire dataset.

Figure 10 summarizes the results of the IP surveys on lines TDIP1 and TDIP2. Rather than showing images of the phase, real and imaginary conductivity, we take advantage of Eqs. 9 and 10 to plot images of the variations in the surface conductivity and electrolytic conductivity between the two sides of the slope. The surface conductivity images directly determined from the IP measurements confirm that the differences in resistivity structure imaged on the large scale survey (Fig. 8) between the two slopes is indeed related to a strong lithological contact with a high surface conductivity (due to high surface area/fine grain size) underlying the NW shallow slope that is absent on the SE leading ridge. In this case, the electrolytic conductivity structure largely mimics the surface conductivity structure, an indication that the fine-grained unit on the NW slope also has a strong difference in porosity and/or pore fluid conductivity relative to the overlying layer and the SW slope. This is reasonable as fine grained sediments (particularly clays) are often characterized by high porosity and elevated dissolved ionic concentrations in the pore fluid due to strong ion exchange from the mineral surface.

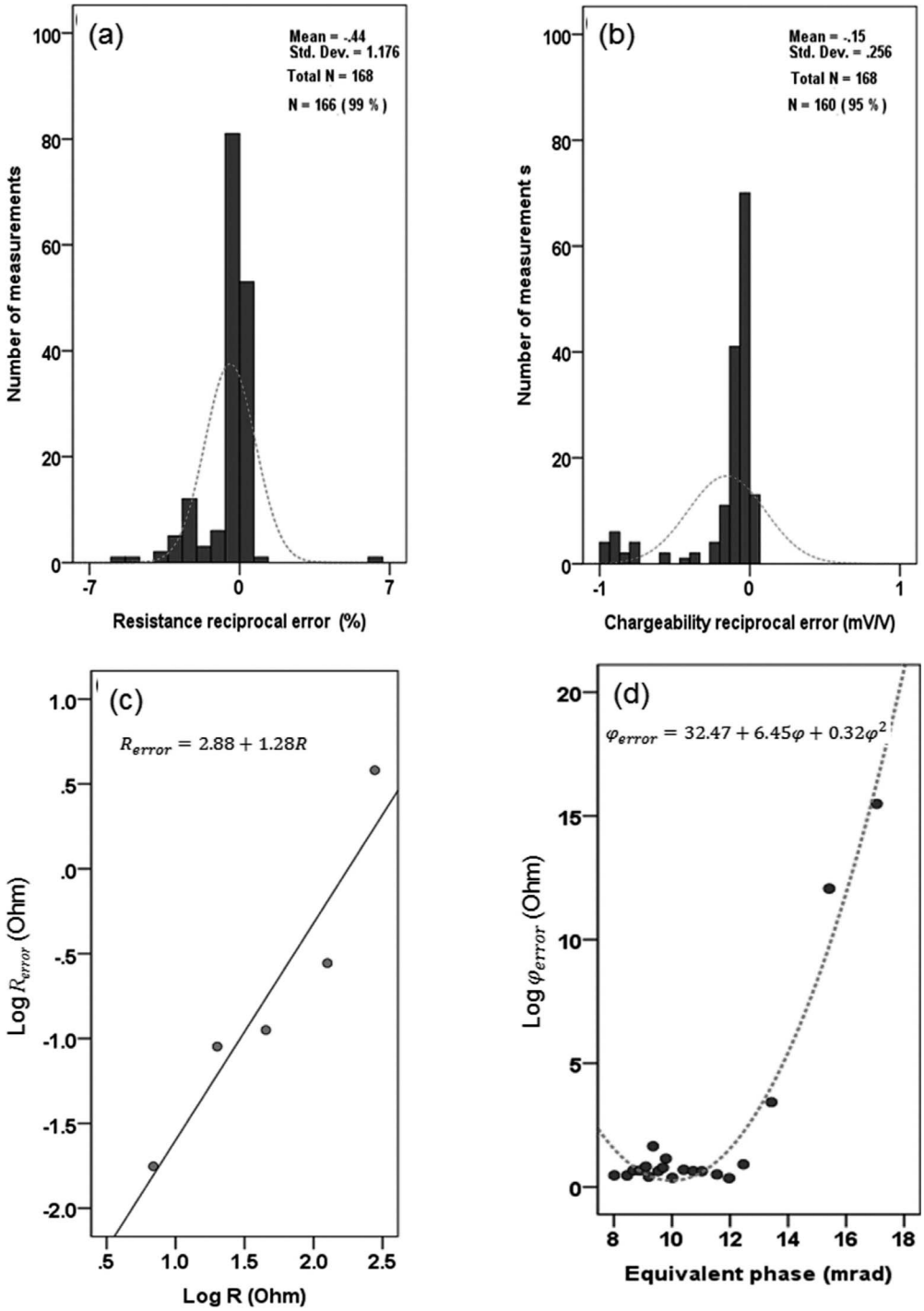

Figure 9. Assessment of errors acquired on TDIP line 1 (see Fig. 8 for location): (a) histogram of percentage resistance reciprocal error variation based on 168 reciprocal measurements; (b) histogram of absolute chargeability reciprocal error based on 168 reciprocal measurements; (c–d) Resistance and chargeability error model applied to invert all 895 measurements, respectively.

Discussion

The acquisition of reliable field-scale IP data using standard time domain systems requires a strong primary voltage (V_p) and low contact resistances at current injection electrodes. Although this critical issue was previously demonstrated by Gazoty *et al*. (2013) using repeatability measurements, we have demonstrated this using reciprocal measurements that are a much more robust measure of field data quality that take into

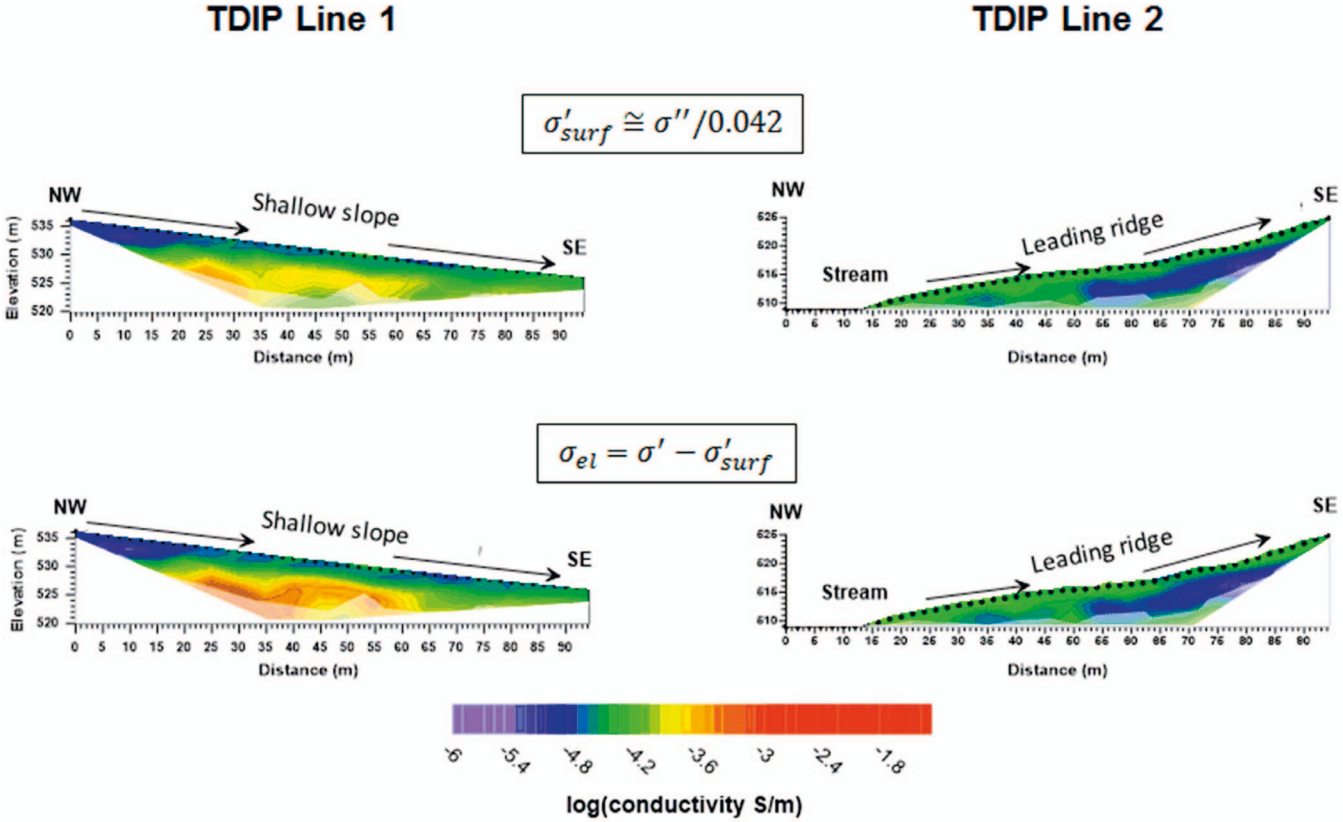

Figure 10. Images of surface conductivity and electrolytic conductivity distributions determined from the IP data shown for TDIP line 1 and TDIP line 2 (see Fig. 8 for line locations). The semi-transparent section of the image at depth represents the structure that is below the DOI and hence inherently uncertain.

account systematic errors. Data acquisition sequences that use potential electrodes separated by a small distance with the dipole pair far from the current injection electrodes (*e.g.,* the Dipole-Dipole array for large separations) will result in a low SNR in the IP measurement. The dependence of IP reciprocal error quality on V_p is clearly demonstrated for the Dipole-Dipole array in Figs. 5 (a)–(c). At our test site, reciprocal errors mostly remain below an arbitrary rejection threshold of 1 mV/V for the low V_p measurements. This is not our experience at electrically conductive sites where a larger portion of the data will have low V_p measurements (often less than 10 mV), and especially at less pristine sites where noise from infrastructure is prevalent. Nested arrays and short offset dipole pairs ($n = 1$ and $n = 2$) provide a strong SNR that is much more critical for IP data acquisition than resistivity data acquisition. At our test site, the IP data acquired with the Wenner α array are not all below our 1 mV/V rejection threshold, an unexpected result given our experiences elsewhere (*e.g.,* at Garner Run). One possible reason for this observation is greater coupling between the wiring connecting the current and potential dipoles in the multicore cable used to acquire data for nested arrays relative to Dipole-Dipole arrays. The use of separate multicore cables for current dipoles and potential dipoles might help reduce such errors (Dahlin and Leroux, 2012), but this is beyond the scope of this study. Such secondary factors illustrate the potential complexity of IP data acquisition relative to resistivity data alone and emphasize the importance of collecting reciprocal data for error analysis whenever possible.

Our results from the test site illustrate that reliable IP data are readily acquired using conventional stainless steel electrodes. We find that the type of electrode has no significant effect on the IP data quality when nested arrays with high SNR are employed (Figs. 5(d)–(f)) and Fig. 7). In contrast, the effect of electrode does become significant as the SNR decreases, clearly demonstrated by the data acquired with the Dipole-Dipole array (Figs. 5(a)–(c)). Consistent with our observations for the Wenner α array, Figs. 5(a)–(c) shows that there is no significant difference in data quality with electrode type for the Dipole-Dipole measurements with high V_p *i.e.,* short dipole offsets. The dependence on electrode material becomes clear for those measurements with a low SNR, *i.e.*, those with $V_p < 30$ mV (Figs. 5(a)–(c)).

Furthermore, the often utilized stainless steel electrode outperforms the Cu-$CuSO_4$ and graphite electrodes. Superior performance of stainless steel electrodes relative to Cu-$CuSO_4$ pots contrary to traditional expectations was first demonstrated by Dahlin *et al*. (2002).

Application of IP surveys to the Garner Run catchment highlights the value of these measurements in constraining the interpretation of the electrical structure of the subsurface relative to using resistivity measurements alone. We demonstrate a presentation of the resistivity/IP data in terms of separate distributions of surface conductivity and electrolytic conductivity that exploits a recently proven linear dependence of the imaginary conductivity determined from IP on the real part of the surface conductivity (Weller *et al*., 2013). This demonstrates how the addition of IP measurements to a resistivity survey can remove the ambiguity between surface conduction and conduction occurring through the interconnected pore space. Within the constraints of inversion artifacts associated with the inversion process, the subsurface distribution of the surface conductivity and electrolytic conductivity is resolved. At this site, surface conduction variations are very significant as demonstrated by the fact that the variability in the surface conductivity is on a similar order of magnitude to the variation in the electrolytic conductivity.

The additional time needed to acquire IP datasets relative to resistivity datasets may deter use of the IP method, particularly when reciprocal measurements are needed to assess data quality and develop error models for the inversion. In the study presented here, only resistivity data were acquired across the large scale roll-along survey across Garner Run. Follow up IP surveys were performed on shorter lines at selected locations identified to confirm the conduction mechanisms associated with the major structural variations identified in the large-scale resistivity survey. Such an approach of focused IP data acquisition to selected targets may present a time efficient use of IP data on constrain resistivity interpretation over larger areas.

Reciprocal errors provide a robust assessment of IP data quality that takes into account the need to switch between electrode pairs on multiple electrode cables such that recorded potentials will inevitably be on electrodes previously used for current injection unless the effort to separate current and voltage recording cables is made (Dahlin and Leroux, 2012). This consideration, plus the additional time considerations in acquiring IP reciprocals, has encouraged some to use repeatability tests to assess IP errors (Gazoty *et al*., 2013). Our philosophy is that IP reciprocal errors are critical to acquire in order to develop appropriate error models for reliable inversion of these challenging measurements where noisy data can quickly lead to unreasonable image structures. We have demonstrated that IP reciprocity should be expected with modern multi-electrode resistivity imaging systems, as previously demonstrated in other field studies where careful IP data were acquired with complete analysis of reciprocals (Flores Orozco *et al*., 2012; Mwakanyamale *et al*., 2012; Slater and Binley, 2006). In the event that it is impractical to acquire a complete set of reciprocals, acquisition of reciprocal data on a representative subset of the entire dataset may be sufficient to quantify the appropriate error model for the site as demonstrated here. The definition of an optimal error model for IP inversion from reciprocal errors is discussed in Flores Orozco *et al*. (2012).

We have limited our discussion to the acquisition of the simplest piece of information from an IP survey, *i.e*., a single measure of the chargeability determined from some integral of the decay curve. Recent advances in the IP method include progress towards acquisition and interpretation of full waveform IP data (*e.g.,* Fiandaca *et al*., 2013, 2012), where the digitized full time domain waveform can be Fourier transformed into the frequency domain, showing the distribution of the IP parameters (typically conductivity magnitude and phase shift) with frequency, or directly inverted for characteristic phenomenological models describing the frequency dependent IP response, *e.g.,* the Cole-Cole model (Fiandaca *et al*., 2012). The data acquisition and data interpretation considerations presented here would equally apply to such efforts to perform a more sophisticated treatment of the IP characteristics of the subsurface.

Conclusions

Signal to noise ratio (SNR) is a primary factor to consider when acquiring IP data with modern multi-electrode imaging systems as demonstrated through robust error analysis based on reciprocity. It outweighs other factors of concern historically considered when acquiring IP data, including for example, the choice of electrode or the need to avoid measuring potentials on electrodes previously used for current injection. These second order factors do become important as the SNR decreases, demonstrated here by a significant dependence of data quality on electrode type for Dipole-Dipole measurements with low primary voltages (less than about 30 mV in this study). Reciprocity is a robust method for characterization of noise in IP datasets

acquired with multi-electrode imaging systems, and important for definition of error models needed to classify errors for the inversion. IP data acquisition comes at considerable additional time expense relative to resistivity data acquisition alone. It may be sufficient to acquired IP reciprocal measurements on a limited subset of the entire dataset to generate robust error models needed for reliable inversion.

An insightful method for interpreting IP data takes advantage of the proven linear relationship between the imaginary conductivity determined from IP measurements and the surface conductivity that contributes to the total conductivity measured with a resistivity survey alone. This utilization of the IP data permits images of the surface conductivity and electrolytic conductivity to be separated. The approach has the potential to significantly improve the geo-electrical interpretation of the subsurface, as demonstrated for a catchment where a contact with an underlying high surface area unit likely restricts vertical transport and promotes quickflow to the stream. Such examples highlight the value of the IP measurement when acquired carefully, and promote the continued development of the technique for environmental investigations.

Acknowledgments

We thank the team at Penn State working at the Susquehanna Shale Hills Critical Zone Observatory (CZO) directed by S. Brantley for help and guidance during field work at Garner Run. Jennifer Williams and Brandon Forsythe provided management and field assistance. The CZO is funded by NSF EAR 12-39285 and 13-31726 in Penn State's Stone Valley Forest. The Forest is supported and managed by the Penn State Forestland Management Office in the College of Agricultural Sciences. We thank Andrew Binley (Lancaster University) for the use of his CR2 code for the inversion of the Garner Run dataset.

References

Archie, G.E., 1942, The electrical resistivity log as an aid in determining some reservoir characteristics: Transactions of the AIME, **146**, 54–62.

Atekwana, E.A., and Atekwana, E.A., 2010, Geophysical signatures of microbial activity at hydrocarbon contaminated sites: A review: Surveys in Geophysics, **31**, 247–283.

Atekwana, E., and Slater, L.D., 2009, Biogeophysics: A new frontier in earth science research: Reviews in Geophysics, **47**, 1–30.

Binley, A., Slater, L.D., Fukes, M., and Cassiani, G., 2005, Relationship between spectral induced polarization and hydraulic properties of saturated and unsaturated sandstone: Water Resources Research, **41**, W12417.

Bleil, D.F., 1953, Induced polarization: A method of geophysical prospecting: Geophysics, **18**, 605–635.

Börner, F.D., 1992, Complex conductivity measurements of reservoir properties: *in* 3rd European Core Analysis Symposium, Paris, 359–386.

Börner, F.D., Schopper, J.R., and Weller, A., 1996, Evaluation of transport and storage properties in the soil and groundwater zone from induced polarization measurements 1: Geophysical Prospecting, **44**, 583–601.

Brantley, S.L., DiBiase, R.A., Russo, T.A., Davis, K.J., Eissenstat, D.M., Dere, A.L., Neal, A.L., Brubaker, K.M., and Arthur, D.K., 2016, Designing a suite of measurements to understand the critical zone: Earth Surface Dynamics, **4**, 211.

Dahlin, T., and Leroux, V., 2012, Improvement in time-domain induced polarization data quality with multi-electrode systems by separating current and potential cables: Near Surface Geophysics, **10**, 545–565.

Dahlin, T., Leroux, V., and Nissen, J., 2002, Measuring techniques in induced polarisation imaging: Journal of Applied Geophysics, **50**, 279–298.

Deceuster, J., Etienne, A., Robert, T., Nguyen, F., and Kaufmann, O., 2014, A modified DOI-based method to statistically estimate the depth of investigation of dc resistivity surveys: Journal of Applied Geophysics, **103**, 172–185.

Fiandaca, G., Auken, E., Christiansen, A.V., and Gazoty, A., 2012, Time-domain-induced polarization: Full-decay forward modeling and 1D laterally constrained inversion of Cole-Cole parameters: Geophysics, **77**, E213–E225.

Fiandaca, G., Ramm, J., Binley, A., Gazoty, A., Christiansen, A.V., and Auken, E., 2013, Resolving spectral information from time domain induced polarization data through 2-D inversion: Geophysical Journal International, **192**, 631–646.

Flores Orozco, A., Kemna, A., and Zimmermann, E., 2012, Data error quantification in spectral induced polarization imaging: Geophysics, **77**, 227–237.

Gazoty, A., Fiandaca, G., Pedersen, J., Auken, E., and Christiansen, A.V., 2013, Data repeatability and acquisition techniques for time-domain spectral induced polarization: Near Surface Geophysics, **11**, 391–406.

Heenan, J., Slater, L.D., Ntarlagiannis, D., Atekwana, E.A., Fathepure, B.Z., Dalvi, S., Ross, C., Werkema, D.D., and Atekwana, E.A., 2015, Electrical resistivity imaging for long-term autonomous monitoring of hydrocarbon degradation: Lessons from the Deepwater Horizon Oil Spill: Geophysics, **80**, B1–B11.

Kemna, A., Binley, A., Cassiani, G., Niederleithinger, E., Revil, A., Slater, L., Williams, K.H., Orozco, A.F., Haegel, F.-H., Hördt, A., Kruschwitz, S., Leroux, V., Titov, K., and Zimmermann, E., 2012, An overview of the spectral induced polarization method for near-surface applications: Near Surface Geophysics, **10**, 453–468.

Kemna, A., Huisman, J.A., Zimmermann, E., Martin, R., Zhao, Y., Treichel, A., Flores Orozco, A., and Fechner, T., 2014, Broadband electrical impedance tomography for subsurface characterization using improved corrections of electromagnetic coupling and spectral regularization: *in* Tomography of the Earth's Crust: From Geophysical Sounding to Real-Time Monitoring, Springer International Publishing.

Koch, K., Kemna, A., Irving, J., and Holliger, K., 2011, Impact of changes in grain size and pore space on the hydraulic conductivity and spectral induced polarization response of sand: Hydrological Earth Systems Science, **15**, 1785–1794.

Koestel, J., Kemna, A., Javaux, M., Binley, A., and Vereecken, H., 2008, Quantitative imaging of solute transport in an unsaturated and undisturbed soil monolith with 3-D ERT and TDR: Water Resources Research, **44**, W12411.

Kruschwitz, S., Binley, A., Lesmes, D., and Elshenawy, A., 2010, Textural controls on low-frequency electrical spectra of porous media: Geophysics, **75**, WA113-WA123.

LaBrecque, D.J., Miletto, M., Daily, W., Ramirez, A., and Owen, E., 1996, The effects of noise on Occam's inversion of resistivity tomography data: Geophysics, **61**, 538–548.

Lesmes, D., and Frye, M., 2001, Influence of pore fluid chemistry on the complex conductivity and induced polarization responses of Berea sandstone: Journal of Geophysical Research, **106**, 4079–4090.

Mansoor, N., and Slater, L., 2007, Aquatic electrical resistivity imaging of shallow-water wetlands: Geophysics, **72**, F211–F221.

Marshall, D.J., and Madden, T.R., 1959, Induced polarization, a study of its causes: Geophysics, **24**, 790–816.

Mwakanyamale, K., Slater, L., Day-Lewis, F., Elwaseif, M., and Johnson, C., 2012, Spatially variable stage-driven groundwater-surface water interaction inferred from time-frequency analysis of distributed temperature sensing data: Geophysical Research Letters, **39**, L06401.

Ntarlagiannis, D., Robinson, J., Soupios, P., and Slater, L., 2016, Field-scale electrical geophysics over an olive oil mill waste deposition site: Evaluating the information content of resistivity versus induced polarization (IP) images for delineating the spatial extent of organic contamination: Journal of Applied Geophysics, **135**, 418–426.

Polyakov, A.C., 1951, Sur la question des potentiels électriques provoqués dans les minerais. Ed. Sci. l'Institut Rech: Géophysiques, Moscou (in French).

Revil, A., Binley, A., Mejus, L., and Kessouri, P., 2015, Predicting permeability from the characteristic relaxation time and intrinsic formation factor of complex conductivity spectra: Water Resources Research, **51**, 6672–6700.

Revil, A., and Florsch, N., 2010, Determination of permeability from spectral induced polarization in granular media: Geophysical Journal International, **181**, 1480–1498.

Revil, A., Kessouri, P., and Torres-Verdín, C., 2014, Electrical conductivity, induced polarization, and permeability of the Fontainebleau sandstone: Geophysics, **79**, D301–D318.

Revil, A., Mendonça, C.A., Atekwana, E.A., Kulessa, B., Hubbard, S.S., and Bohlen, K.J., 2010, Understanding biogeobatteries: Where geophysics meets microbiology: Journal of Geophysical Research, **115**, G00G02.

Seigel, H., Nabighian, M., Parasnis, D.S., and Vozoff, K., 2007, The early history of the Induced Polarization method: The Leading Edge, **26**, 312–321.

Slater, L., and Binley, A., 2006, Synthetic and field-based electrical imaging of a zero valent iron barrier: Implications for monitoring long-term barrier performance: Geophysics, **71**, B129–B137.

Slater, L., Binley, A., Daily, W., Johnson, R., and Binley, A., 2000, Cross-hole electrical imaging of a controlled saline tracer injection: Journal of Applied Geophysics, **44**, 85–102.

Slater, L.D., and Lesmes, D., 2002, IP interpretation in environmental investigations: Geophysics, **67**, 77–88.

Sumi, F., 1959, Geophysical exploration in mining by Induced Polarization: Geophysical Prospecting, **7**, 300–310.

Telford, W.M., Geldart, L.P., and Sheriff, R.E., 1990, Applied Geophysics—2nd ed.: Cambridge University Press, Cambridge.

Titov, K., Tarasov, A., Ilyin, Y., Seleznev, N., and Boyd, A.S.M., 2010, Relationships between induced polarization relaxation time and hydraulic properties of sandstone: Geophysical Journal International, **180**, 1095–1106.

Vacquier, V., Holmes, C.R., Kintzinger, P.R., and Lavergne, M., 1957, Prospecting for ground water by induced electrical polarization: Geophysics, **22**, 660–687.

Van Dam, R.L., Simmons, C.T., Hyndman, D.W., and Wood, W.W., 2009, Natural free convection in porous media: First field documentation in groundwater: Geophysical Research Letters, **36**, L11403.

Vinegar, H.J., and Waxman, M.H., 1984, Induced polarization of shaly sands: Geophysics, **49**, 1267–1287.

Wait, J., 1959, Overvoltage research and geophysical applications: Pergamon Press, London, New York.

Weller, A., and Slater, L., 2012, Salinity dependence of complex conductivity of unconsolidated and consolidated materials: Comparisons with electrical double layer models: Geophysics, **77**, 185–198.

Weller, A., Slater, L., and Nordsiek, S., 2013, On the relationship between induced polarization and surface conductivity: Implications for petrophysical interpretation of electrical measurements: Geophysics, **78**, 315–325.